Gas-phase spin relaxation of ^{129}Xe

B. C. Anger,[1] G. Schrank,[1] A. Schoeck,[1] K. A. Butler,[1] M. S. Solum,[2] R. J. Pugmire,[3] and B. Saam[1,*]
[1]*Department of Physics, University of Utah, Salt Lake City, Utah 84112, USA*
[2]*Department of Chemistry, University of Utah, Salt Lake City, Utah 84112, USA*
[3]*Department of Chemical Engineering, University of Utah, Salt Lake City, Utah 84112, USA*
(Received 30 May 2008; published 8 October 2008)

We have completed an extensive study of ^{129}Xe longitudinal spin relaxation in the gas phase, involving both intrinsic and extrinsic mechanisms. The dominant intrinsic relaxation is mediated by the formation of persistent Xe_2 van der Waals dimers. The dependence of this relaxation on applied magnetic field yields the relative contributions of the spin-rotation and chemical-shift-anisotropy interactions; the former dominates at magnetic fields below a few tesla. This relaxation also shows an inverse quadratic dependence on temperature T; the maximum low-field intrinsic relaxation for pure xenon at room temperature (measured here to be 4.6 h, in agreement with previous work) increases by $\approx$60% for $T=100\,^{\circ}$C. The dominant extrinsic relaxation is mediated by collisions with the walls of the glass container. Wall relaxation was studied in silicone-coated alkali-metal-free cells, which showed long (many hours or more) and robust relaxation times, even at the low magnetic fields typical for spin-exchange optical pumping ($\approx$3 mT). The further suppression of wall relaxation for magnetic fields above a few tesla is consistent with the interaction of ^{129}Xe with paramagnetic spins on or inside the surface coating. At 14.1 T and sufficiently low xenon density, we measured a relaxation time $T_1=99$ h, with an inferred wall-relaxation time of 174 h. A prototype large storage cell (12 cm diameter) was constructed to take advantage of the apparent increase in wall-relaxation time for cells with a smaller surface-to-volume ratio. The measured relaxation time in this cell at 3 mT and 100 °C was 5.75 h. Such a cell (or one even larger) could be used to store many liters of hyperpolarized ^{129}Xe produced by a flow-through polarizer and accumulator for up to three times longer than currently implemented schemes involving freezing xenon in liquid nitrogen.

DOI: 10.1103/PhysRevA.78.043406 PACS number(s): 33.25.+k, 32.80.Xx, 34.35.+a, 82.56.−b

I. INTRODUCTION

Noble-gas isotopes having nonzero nuclear spin may be optically polarized to levels approaching unity via the technique of spin-exchange optical pumping (SEOP) [1,2], whereby the typically weak signal generated by nuclear moments is enhanced by several orders of magnitude. Even after several decades of work by many groups, hyperpolarized gases continue to be studied and applied in a wide variety of magnetic-resonance experiments; we cite a few recent examples [3–5]. In a typical implementation, circularly polarized laser light is incident on a glass cell containing an excess amount of an alkali metal (usually Rb), the noble gas, and a small quantity of nitrogen to promote collisional deexcitation of the excited states [6] generated by resonant absorption of the laser light by the alkali-metal vapor at the first principal (D_1) electric-dipole transition. (This corresponds to a wavelength of 795 nm for Rb.) The alkali-metal vapor density is controlled by adjusting the cell temperature from room temperature up to $\approx$500 K. The selection rule for absorption of circularly polarized light and collisional mixing of the excited-state magnetic sublevels lead to rapid and efficient spin polarization of the valence electron of the alkali-metal vapor. Collisions with noble-gas atoms then lead to an exchange of angular momentum between the alkali-metal electron and the noble-gas nucleus. The time-dependent buildup of nuclear polarization $P_N(t)$ in such a sample that occurs while the laser is on is given by[1]

$$P_N(t)=\langle P_A\rangle\frac{\gamma_{se}}{\gamma_{se}+\Gamma}[1-e^{-(\gamma_{se}+\Gamma)t}], \tag{1}$$

where $\langle P_A\rangle$ is the time- and volume-averaged alkali-metal polarization, γ_{se} is the spin-exchange rate, and Γ is the longitudinal relaxation rate of the noble gas due to to all other mechanisms. It is clear from Eq. (1) that Γ limits the ultimate nuclear polarization for a fixed value of γ_{se}, the latter being limited by available laser power and the photon efficiency (the number of polarized nuclei produced per photon absorbed in the cell volume) [8] for a given alkali-metal-noble-gas pair and laser and cell geometry, whereby one generally maintains $\langle P_A\rangle$ close to unity. An understanding of the mechanisms responsible for the relaxation rate Γ is thus essential to the efficient production of hyperpolarized gases.

While SEOP is typically used to polarize either of the stable spin-1/2 noble-gas isotopes, ^{3}He and ^{129}Xe, we are concerned in this work specifically with the relaxation mechanisms that limit the polarization of ^{129}Xe. The relaxation rate Γ may be written [9]

*saam@physics.utah.edu

[1]In Eq. (1) we have ignored the anomalous excess relaxation that scales with alkali-metal density recently observed for SEOP of ^{3}He [7].

$$\Gamma = \Gamma_t + \Gamma_p + \Gamma_g + \Gamma_w, \tag{2}$$

where $\Gamma_i = \Gamma_t + \Gamma_p$ is the intrinsic rate due to the sum of contributions from transient and persistent Xe_2 dimers; and $\Gamma_e = \Gamma_g + \Gamma_w$ is the extrinsic rate due to the sum of contributions from atomic diffusion through gradients in the applied magnetic field [10,11] and interactions with the cell surface (wall relaxation). In most cases involving SEOP of xenon, some combination of Γ_p and Γ_w dominates the relaxation. For xenon densities $[Xe] > 0.1$ amagat, Γ_g is usually negligible [9], although there is a size limitation for hyperpolarized-xenon storage cells in a given Helmholtz geometry due to this mechanism (see Sec. IV E). For $[Xe] \geqslant 0.1$ amagat, Γ_t sometimes makes a small but non-negligible contribution to the total relaxation rate.

We have performed extensive NMR measurements of Γ on ^{129}Xe gas as a function of temperature and magnetic field that serve to separate and quantify the contributions of persistent-dimer relaxation and wall relaxation. Based on the present and previous work [9,12,13], we have developed a semiempirical formula for the intrinsic relaxation rate Γ_i of ^{129}Xe as a function of xenon density [Xe] (amagats), applied magnetic field B_0 (T), and gas composition. This formula applies at room temperature in the fast-fluctuation limit (defined below), i.e., for $[Xe] \gtrsim 0.3$ amagat at all reasonable values of B_0 and for much lower xenon densities when $B_0 \lesssim 1$ T:

$$\Gamma_i = \frac{[Xe]}{56.1\ \text{h}} + \frac{1}{4.59\ \text{h}}[1 + (3.65 \times 10^{-3})B_0^2]\left(1 + r\frac{[B]}{[Xe]}\right)^{-1}, \tag{3}$$

where the first term is due to transient dimers [13] and the second (usually dominant) term is due to persistent dimers; $[B]$ is the density of a second gas in the mixture, and $r \equiv k_B/k_{Xe}$ is the ratio of the persistent-dimer breakup coefficient for the second gas to that for xenon. We have measured $r = 0.51$ for nitrogen [9], which, along with helium, is most often present with xenon in SEOP situations. For helium, Chann *et al.* [12] have measured $r = 0.25$. In the present work we observed a $1/T^2$ temperature dependence in the range 293–373 K for the persistent-dimer term at $B_0 = 8.0$ T, but the model for this dependence is not well understood (see Secs. II B and IV C). We have neglected here relaxation due to persistent dimers of xenon with other atoms, which generally have weaker binding and have been shown to contribute negligibly to relaxation [12]; we have also neglected relaxation due to binary collisions with other molecules besides xenon—to our knowledge, only relaxation due to paramagnetic oxygen has been measured [14]. The uncertainty in the relaxation time calculated from Eq. (3) is about 10%.

Longitudinal relaxation also limits the accumulation and storage of hyperpolarized gases. Attaining storage times of several hours or more is directly relevant to applications such as magnetic resonance imaging (MRI), where the gas must often be transported to the MRI scanner with minimal polarization loss. In the case of ^{129}Xe, a relatively long longitudinal relaxation time $T_1 \equiv \Gamma^{-1}$ is also important for the accumulation stage in a flow-through xenon polarizer [15,16], the current state-of-the-art scheme for the versatile production of liter quantities of highly polarized ^{129}Xe for any application. In these devices, a gas mixture lean in xenon is passed continuously through a glass cell, in which it is polarized by SEOP with a laser, and subsequently frozen as a polycrystalline solid at 77 K in a liquid-nitrogen trap. This basic scheme has proven effective in dealing with the inherently low (7%) Rb-Xe spin-exchange efficiency, i.e., the rate at which angular momentum is transferred to the noble-gas nucleus divided by the rate at which it is lost by the alkali-metal atoms [17]. The source of this low efficiency is the strong spin-rotation interaction of the rubidium valence electron with the electron cloud of the xenon atom, whereby $\langle P_A \rangle$ begins to plummet for xenon densities $[Xe] > 1$ amagat. Hence, ^{129}Xe (unlike ^3He) is not readily polarized in large batches at high density. Cryogenic accumulation of xenon as it flows out of the polarizing cell serves two purposes. First, it separates out the other gases, typically nitrogen and helium, making it possible to prepare pure xenon samples. Second, since most or all of the polarization survives the phase transition [16,18], large quantities of hyperpolarized xenon can be accumulated from the low-density flow and stored for times on the order of $T_1 \approx 2.5$ h at 77 K in an applied magnetic field $B_0 \geqslant 0.1$ T [19] before being revolatilized. This method evolved, in part, because of the reliable 2.5 h storage time, although it became clear in later work that the gas must be quickly and completely frozen to 77 K [16]; at higher temperatures, particularly those approaching the xenon melting point (161 K), relaxation rates increase dramatically due to vacancy diffusion in the solid [20], resulting in polarization losses in the freeze-and-thaw cycle.

Accumulation and storage of hyperpolarized xenon near room temperature in the gas phase is desirable in that it would eliminate the need for large magnetic fields, the cryogenic apparatus, and freeze-and-thaw cycles. The historical problem with this approach has been that ^{129}Xe gas-phase relaxation is relatively fast and notoriously irreproducible, whereby wall relaxation plays a crucial role. Some progress was made in understanding wall interactions, particularly in cells treated with silane- or siloxane-based surface coatings in fields on the order of 1 mT [21,22], where $T_1 = 20–60$ min was observed. Others observed $T_1 > 3$ h for some coated cells at 9.4 T, an indication that wall relaxation is suppressed at high field [13,23]. These studies all had in common relatively small cells (1–3 cm diameter) that contained macroscopic amounts of rubidium along with the coating, meaning that the gas was polarized by SEOP in the same cell in which T_1 was subsequently measured. While it is well known that ^3He relaxation on uncoated glass is reliably suppressed by the presence of alkali metal [24–27], this is apparently not the case for ^{129}Xe, where in fact, the interaction of the alkali metal with the surface coating, particularly when heated to 100 °C or more during SEOP can lead to erratic and generally increasing relaxation rates [9]. Evidence presented here and in our previous work [9] strongly indicates that wall relaxation in xenon cells is not relaxation-site limited at the usual SEOP densities, i.e., xenon atoms are not inhibited from interacting with wall sites due to their occupation by other xenon atoms. Hence, in the regime for

which the wall contribution to T_1 is long compared to the mean time for a xenon atom to diffuse across the cell (easily realized in all of our experiments and most others), the wall-relaxation rate is independent of [Xe] and depends linearly on the surface-to-volume ratio S/V. This reasoning has led us to take a closer look at larger-diameter coated cells containing no alkali metal as a way of reducing the ^{129}Xe gas-phase wall-relaxation rate.

Several years ago, Chann *et al.* first demonstrated gas-phase ^{129}Xe relaxation due to persistent Xe_2 dimers [12]. These van der Waals molecules are formed in three-body collisions and have a mean lifetime $\tau_p \approx 1$ ns for $[Xe] \approx 1$ amagat [9,12] before being destroyed by another collision. The maximum relaxation time for a pure xenon sample due to this mechanism alone was shown to be ≈ 4 h and independent of [Xe] for low applied magnetic field B_0 (a few milliteslas). The density independence arises both because the fraction of xenon atoms bound in molecules and the molecular formation and breakup rate τ_p^{-1} have the same linear dependence on [Xe], and because the fast-fluctuation limit $\Omega^2\tau_p^2 \ll 1$, where Ω is the ^{129}Xe Larmor frequency, holds for all reasonable values of [Xe] and $B_0 < 1$ T; see Eq. (4) below. This density independence effectively mimics wall relaxation, and it has undoubtedly confounded some earlier work in measuring Γ_w, particularly since the minimum intrinsic rate Γ_p is much larger than previously believed [13,28]. Our group recently verified and extended this work at low [Xe] and $B_0 = 8.0$ T, which straddles the fast- and slow-fluctuation regimes [9]. We showed that persistent-dimer relaxation is strongly suppressed at this field for sufficiently low xenon densities ($\lesssim 0.1$ amagat).

Continued progress in the understanding of gas-phase relaxation of ^{129}Xe is paving the way for significant improvements in cell performance with regard to hyperpolarized gas production, accumulation, storage, and transport for the various applications. In this work, we have extended our study of this relaxation to a wide range of applied magnetic fields and temperatures, with an eye toward a large-diameter ($\geqslant 20$ cm) coated cell that could store many liters of hyperpolarized xenon with a $T_1 \geqslant 7$ h in an applied magnetic field of ≈ 3 mT, tripling the storage time of solid xenon at 77 K and eliminating the need for high-field cryogenic accumulation. The work is divided into three main parts. (1) The study of the magnetic suppression of the persistent-dimer mechanism in a range of magnetic fields from 1.5 to 14.1 T. This data allowed us to deduce the relative strength of the spin-rotation (SR) and chemical-shift-anisotropy (CSA) interactions via the B_0^2 dependence of the CSA contribution. This, in turn, generates an independent estimate for the maximum low-field pure-xenon relaxation time of $T_1 = 4.6$ h. (2) The study of wall relaxation over the same range of B_0 and further on down to 3 mT. This is made possible by a thorough understanding of the persistent-dimer mechanism with which wall relaxation often competes. Wall-relaxation times in our alkali-metal-free coated cells varied from ≈ 10 h at 3 mT to >100 h at 14.1 T, suggesting a high-field decoupling of a wall mechanism that has to do with interactions of ^{129}Xe atoms with unpaired electrons at the surface or inside of the coating [21]. (3) The study of the temperature dependence of the persistent-dimer rate Γ_p in the fast-fluctuation limit in the range of 20–100 °C. The observed inverse-square dependence of Γ_p on temperature T results in an increase of $\approx 60\%$ in the relaxation time due to persistent dimers at 100 °C compared to room temperature.

II. THEORY

A. Persistent-dimer relaxation

Intrinsic longitudinal relaxation of ^{129}Xe gas in the SEOP regime of pressure and temperature is dominated by the spin-rotation [29] and chemical-shift-anisotropy [30,31] interactions modulated by the formation and breakup of persistent Xe_2 dimers in three-body collisions. The theory is discussed in detail in Refs. [9,12]. In brief, the persistent-dimer relaxation rate is given by

$$\Gamma_p = (2\mathcal{K}[\mathrm{Xe}])(M^{\mathrm{SR}} + M^{\mathrm{CSA}})\left(\frac{\tau_p}{1+\Omega^2\tau_p^2}\right), \tag{4}$$

where $\mathcal{K} \equiv [\mathrm{Xe}_2]/[\mathrm{Xe}]^2$ is the chemical equilibrium coefficient; and M^{SR} and M^{CSA} are the mean-squared interaction strengths (second moments) of the SR and CSA interactions, respectively. We refer to τ_p^{-1} as the breakup rate for persistent dimers, although it is more generally the rate of all collisional processes in which the angular momentum of the molecule is appreciably changed. The three factors on the right-hand side of Eq. (4) correspond, respectively, to the fraction of xenon atoms bound in molecules, the total mean-squared interaction strength, and the power spectrum of collision-induced field fluctuations. In the approximation (valid here) that equilibrium vastly favors xenon monomers, the dimer fraction is linearly dependent on the concentration of xenon only; whereas the breakup rate τ_p^{-1} depends linearly on the concentration of all gas species present.

Neglecting the transient-dimer and gradient-relaxation terms in Eq. (2), we can reparamaterize Eq. (4) and add to it the wall-relaxation rate Γ_w to obtain the total relaxation rate:

$$\Gamma([G]) = \Gamma_w + 2\mathcal{K}(M^{\mathrm{SR}} + M^{\mathrm{CSA}})\left(\frac{\alpha k_\alpha [G]^2}{k_\alpha^2[G]^2 + \Omega^2}\right), \tag{5}$$

where $[G]$ is the total gas density, $\alpha \equiv [\mathrm{Xe}]/[G]$ is the xenon concentration, and k_α is the molecular breakup coefficient for the particular gas composition. In this work, nitrogen is the only other gas in the mixture, and

$$\frac{1}{\tau_p} = k_\alpha[G] = k_{\mathrm{Xe}}[\mathrm{Xe}] + k_{\mathrm{N}}[\mathrm{N}_2], \tag{6}$$

where k_{Xe} and k_{N} are the breakup coefficients for xenon and nitrogen as third bodies, respectively.

At high gas densities, in the fast-fluctuation limit $\Omega^2 \ll k_\alpha^2[G]^2$ of Eq. (5), the persistent-dimer relaxation rate is independent of $[G]$ for a given gas composition, as first observed by Chann *et al.* [12] for $B_0 = 2.0$ mT and also by our group for $B_0 = 8.0$ T [9]. At lower densities the rate is suppressed due to the increasing relevance of the Ω^2 term in Eq. (5). Whereas M^{SR} is independent of the applied field B_0 [29], M^{CSA} is proportional to B_0^2. Hence, acquiring a set of relaxation curves as a function of $[G]$ that are fitted to Eq. (5),

where each curve is at one of several values of B_0, allows M^{SR} to be separated from M^{CSA}.

B. Expected temperature dependence

Each of the three factors in Eq. (5) has a nontrivial dependence on temperature T. The temperature dependence of the persistent-dimer fraction comes through the chemical equilibrium coefficient $\mathcal{K}$, given by [32]

$$\mathcal{K} = \frac{1}{2}\left(\frac{h^2}{2\pi\mu kT}\right)^{3/2} Z, \tag{7}$$

where h is the Planck constant, k is the Boltzmann constant, $Z=\Sigma_i e^{-E_i/kT}$ is the sum over all of the internal states of the Xe_2 dimer, and μ is its reduced mass. The portion of this expression that multiplies Z is the ratio of the translational partition function for a single dimer to that for two free atoms in the classical high-temperature and low-density limit. We argue here that for our temperature range, Z should be approximately linear in T. The energy of the ith state is

$$E_i = E_e + E_{ri} + E_{vi}, \tag{8}$$

where $E_e/k=-283$ K is the potential well depth of the xenon dimer [33], and E_{ri} and E_{vi} are the rotational and vibrational energies of the ith state. The internal partition function $Z=Z_eZ_rZ_v$ is the product of partition functions corresponding to electronic excitations, rotations, and vibrations. Over the temperature range we have examined, 295–395 K, $Z_e=e^{-E_e/kT}$ follows approximately a $1/T$ dependence. The characteristic rotational energy spacing $h^2/2\Theta \ll kT$, where Θ is the rotational inertia of the xenon dimer; hence, the sum over rotational states can be reasonably approximated as an integral, leading to [32]

$$Z_r = \frac{2\Theta kT}{\hbar^2}. \tag{9}$$

The corresponding energy spacing for the vibrational levels is $\hbar\omega/k \approx 29$ K, derived from approximating the xenon-dimer potential in Ref. [33] as ideally harmonic. The partition function Z_v is thus estimated as [32]

$$Z_v = \frac{e^{-\hbar\omega/2kT}}{1-e^{-\hbar\omega/kT}}. \tag{10}$$

Although the energy spacing only marginally satisfies the condition $\hbar\omega \ll kT$, Eq. (10) is very nearly linear in T in our temperature range. Hence, when we multiply the $T^{-3/2}$ dependence of the kinetic factor in Eq. (7) by the linear dependence for Z, we expect the overall temperature dependence for the equilibrium coefficient $\mathcal{K}$ to be approximately $T^{-1/2}$. As a check on this analysis, using $R_0=4.38$ Å as the equilibrium separation of the xenon dimer [33] and $\mu=1.07\times10^{-25}$ kg, we combine Eqs. (9) and (10) with the Boltzmann factor for Z_e and calculate $\mathcal{K}=204$ Å^3 at 297 K using Eq. (7). A more careful calculation using a Fourier gridding method done by Chann *et al.* [12] yielded $\mathcal{K}=230$ Å^3 at 297 K. These values correspond to a dimer fraction of 1% for [Xe]=1 amagat.

The temperature dependence of the mean-squared interaction strengths is well known to be linear in T for the SR interaction, because it depends on the square of the molecular angular momentum, which obeys equipartition in the high-temperature limit [29]. The CSA interaction depends on the orientation of the angular momentum with respect to the applied field and so is temperature independent [31]. Classically, τ_p is inversely proportional to the mean relative velocity of the gas molecules and to the breakup cross section: the former is proportional to $T^{1/2}$ and the latter likely increases with temperature, as the energy delivered by the third body to the molecule in a collision will increase linearly with T, but the exact dependence is determined by the details of the intermolecular potentials involved.

To estimate the total temperature dependence for Γ_p, we treat here only the SR interaction in the fast-fluctuation limit, $\Omega^2\tau_p^2 \ll 1$, relevant to high-density xenon storage cells in small magnetic fields. The product $\mathcal{K}M^{\mathrm{sr}}\tau_p$ appears in this limit, and the dependences deduced for each of these three factors cancel. Thus, we expect little or no temperature dependence to the relaxation rate Γ_p, apart from whatever dependence there is to the breakup cross section. The observed T^{-2} dependence in our data (discussed below) is thus somewhat surprising.

III. EXPERIMENTAL PROCEDURE

Many of the procedures described here are very similar or identical to those described in detail in our previous work [9]. Most of the measurements of the longitudinal relaxation time T_1 for ^{129}Xe in xenon gas were done in a single borosilicate-glass (Pyrex) "measurement" cell, designated 113B. It is a 6.7-cm-diameter sphere connected via a 10 cm length of capillary (0.5 mm diameter) to a glass valve and sidearm used for evacuation and refilling. A 4 cm length of 6 mm glass tubing (the stem) extends from the sphere opposite the capillary entrance. The cell contains no alkali metal, but the interior was coated with dimethyldichlorosilane, which inhibits wall relaxation in a manner similar to silicone coatings previously introduced [21,22].

Hyperpolarized xenon was usually generated in one of several "pumping" cells, which have a geometry similar to the measurement cells and also contain Rb metal for SEOP. Our high-vacuum gas-handling system [34] is used to measure cell volumes, evacuate cells, and to refill pumping cells with a precise mixture of xenon (isotopically enriched to 86%; Spectra Gases, West Branchburg, NJ) and nitrogen. Unless otherwise noted, the xenon concentration $\alpha=0.91\pm0.02$ throughout this work, where the error reflects variation in multiple preparations of the mixture in the pumping cells. The effects of varying α are consistent with the theory presented above and were studied previously [9,12].

Xenon gas, polarized by SEOP to ≈10% in a pumping cell, was then transferred (at the known value of α) to the measurement cell using a glass transfer manifold and mechanical vacuum pump for evacuating dead space. In the case of the 1.5 and 8.0 T fields, the cell was immediately inserted into a NMR probe and the probe assembly was inserted into the magnet. In the case of the 4.7 and 14.1 T fields, the polarized measurement cell was transported from

the Department of Physics across campus in a portable 2 mT battery-powered solenoidal coil to an NMR facility in the Department of Chemistry. (Less than 10% of the magnetization was lost during transport.) All magnets (with the exception of the 1.5 T magnet) had a wide-bore (89 mm diameter) vertical configuration. The probes were capacitively tuned saddle coils (one to two turns) placed along the stem of the cell; the respective resonance frequencies corresponded to the ^{129}Xe gyromagnetic ratio of 11.8 MHz/T. In the 1.5 T field (provided by a 30-cm-diameter horizontal-bore imaging magnet), the cell was situated horizontally at the magnet isocenter with a surface-coil probe placed underneath it.

NMR measurements were conducted with an Aries (Tecmag) spectrometer with a homebuilt rf section (1.5 and 8.0 T), Chemagnetics CMX200 (4.7 T), and Varian Infinity-plus 600 (14.1 T). For measurements above room temperature, the 8.0 T probe was insulated and heated with air flowing across a filament heater located away from the magnet. In addition, several low-field ($B_0 \approx 3$ mT) measurements were made using a homebuilt low-frequency spectrometer [35], whereby the cell and NMR probe were placed in an oven (similarly heated with flowing hot air) located at the isocenter of a Helmholtz pair. In all cases the longitudinal relaxation rate Γ was measured by periodic acquisition of a free-induction decay (FID) induced by a single rf pulse. A negligible fraction of the magnetization was destroyed by each pulse. Either the height or the area under the the peak of each Fourier-transformed FID was plotted as a function of time and a least-squares fit was used to extract Γ.

We note that the use of some small amount of nitrogen is necessary for efficient optical pumping [6]; thus, most of our measurements were done with a specific value of $\alpha < 1$. In the course of this work, our laboratory completed the construction of a flow-through xenon polarizer and accumulator, with which we can produce samples of pure hyperpolarized xenon ($\alpha = 1$). We used this device for a few later experiments, as noted below. For technical reasons, the pumping-cell scheme still provides the most precise measurement of total gas density and xenon concentration needed for many of these experiments. The polarizer and accumulator was used for measurements that did not require precise knowledge of gas density.

IV. RESULTS AND DISCUSSION

A. Field dependence at room temperature

The relaxation rate Γ was measured as a function of total gas density $[G]$ for the four different magnetic fields. The data were fitted in each case to Eq. (5) using the appropriate value of the Larmor frequency Ω, with the wall-relaxation rate Γ_w and the interaction-strength term $2\mathcal{K}(M^{\mathrm{SR}}+M^{\mathrm{CSA}})$ extracted as free parameters; see Table I. Since the xenon concentration α and, hence, the breakup coefficient k_α are field independent, the value

$$k_\alpha = (3.54 \pm 0.28) \times 10^{-10}\ \mathrm{cm}^3/\mathrm{s} \qquad (11)$$

was determined from a global fit to the four data sets, and this value was then used as a fixed parameter for each of the fits to the individual data sets. The plot in Fig. 1 shows the persistent-dimer rate $\Gamma_p = \Gamma - \Gamma_w$ plotted vs $[G]$ for all four fields along with the respective best fits. The errors in the free parameters were, in general, underestimated by our nonlinear fitting routines and had to be handled with some care. They were determined for a given field and temperature by allowing k_α to vary over its error range and observing the effect in the fit on $2\mathcal{K}(M^{\mathrm{SR}}+M^{\mathrm{CSA}})$ and Γ_w.

TABLE I. Free parameters extracted from the fits of the data shown in Fig. 1 to Eq. (5). Errors are given in parentheses for the least significant figure (s).

B_0 (T)	$2\mathcal{K}(M^{\mathrm{SR}}+M^{\mathrm{CSA}})$ (10^{-14} cm^3/s^2)	Γ_w (10^{-6} s^{-1})
1.5	2.02(17)	18.5(9)
4.7	2.53(14)	4.1(5)
8.0	2.87(15)	3.70(8)
14.1	3.86(9)	1.60(19)

The effect of the CSA interaction is shown in Fig. 1 by the monotonic increase of the asymptotic high-density rate with increasing magnetic field. To determine the relative contributions of the SR and CSA interactions, the parameter $2\mathcal{K}(M^{\mathrm{SR}}+M^{\mathrm{CSA}})$ is plotted vs the square of the applied field B_0 in Fig. 2. The data are consistent with a linear B_0^2 dependence. The slope and intercept from a linear least-squares fit yield, respectively,

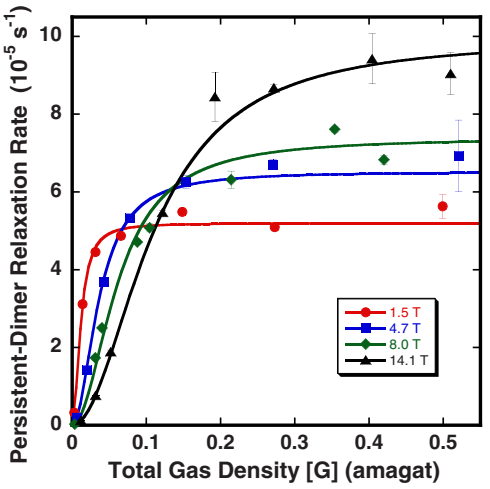

FIG. 1. (Color online) Plot of the room-temperature ^{129}Xe persistent-dimer relaxation rate vs total gas density for a fixed xenon concentration $\alpha = 0.91$ at four different applied magnetic fields. The wall relaxation rate Γ_w and the product $2\mathcal{K}(M^{\mathrm{SR}}+M^{\mathrm{CSA}})$ are extracted from fits of the measured relaxation rates $\Gamma([G])$ to Eq. (5) for each field (see Table I). The corresponding value of Γ_w has been subtracted from all the data sets in this plot to show clearly the behavior of the persistent-dimer rate Γ_p. The high-density fast-fluctuation limit results in a density-independent relaxation rate (asymptote) that increases with field due to the increasing strength of the CSA interaction (see Fig. 2); the magnetic suppression of the persistent-dimer mechanism with decreasing density starts at higher densities and happens more gradually for higher fields. The field-independent molecular breakup coefficient $k_\alpha = (3.54 \pm 0.28) \times 10^{-10}$ cm^3/s was extracted from a global fit to all four data sets.

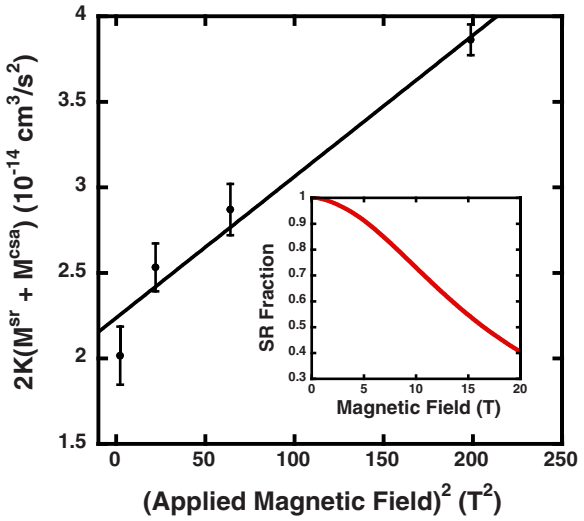

FIG. 2. (Color online) Plot of $2\mathcal{K}(M^{\mathrm{SR}}+M^{\mathrm{CSA}})$ extracted from the fits in Fig. 1 (see Table I) vs the square of the applied magnetic field B_0 at room temperature. A linear fit to the data yields the relative contributions of the SR and CSA interactions as a function of B_0, as given in Eqs. (12) and (13), where the intercept is proportional to the field-independent spin-rotation second moment M^{SR}, which can then be used to deduce the limiting low-field pure-xenon relaxation rate due to persistent dimers; see Sec. IV B. The inset graph shows the fraction of the the total second moment due to SR as a function of B_0; the interactions contribute equally at $B_0 \approx 16.5$ T.

$$2\mathcal{K}M^{\mathrm{CSA}} = [(8.26 \pm 0.73) \times 10^{-17}\ \mathrm{cm^3/s^2\ T^2}]B_0^2, \quad (12)$$

$$2\mathcal{K}M^{\mathrm{SR}} = (2.24 \pm 0.10) \times 10^{-14}\ \mathrm{cm^3/s^2}. \quad (13)$$

The inset graph to Fig. 2 shows the fraction of the the total second moment that is due to the SR interaction as a function of B_0; the SR and CSA interactions contribute equally at a crossover field $B_0 \approx 16.5$ T. A factor accounting for faster relaxation at higher fields appears in the intrinsic relaxation formula [Eq. (3)]. Moudrakovski *et al.* [13] made a similar measurement at very high xenon densities (>30 amagats), in the transient-dimer regime, and found that the SR and CSA interactions contribute equally for $B_0=12$ T. Although our measurement was made at much lower density in the persistent-dimer regime, there is no apparent reason that the crossover field should be different in the two cases. In general, the crossover field should increase with temperature, due to the linear temperature dependence of M^{SR} [29].

B. Minimum low-field relaxation rate

The result in Eq. (13) can be used to calculate the density-independent persistent-dimer relaxation rate for pure xenon gas in the high-density low-field limit, where only the SR interaction contributes; this is almost always the relevant regime for SEOP. Here we follow the notation originally introduced by Chann *et al.* [12] for this characteristic limiting rate:

$$\Gamma_{\mathrm{vdW}}^{\mathrm{Xe}} = \frac{2\mathcal{K}M^{\mathrm{SR}}}{k_{\mathrm{Xe}}}. \quad (14)$$

We use the value of k_α in Eq. (11) and the value of the nitrogen breakup coefficient $k_{\mathrm{N}}=(1.9\pm0.2)\times10^{-10}$ cm^3/s measured in our previous work [9] in Eq. (6) to calculate $k_{\mathrm{Xe}}=(3.70\pm0.31)\times10^{-10}$ cm^3/s. This represents only a small correction to our value of k_α, since our samples are over 90% xenon. Finally, using Eqs. (13) and (14), we obtain

$$\Gamma_{\mathrm{vdW}}^{\mathrm{Xe}} = (6.05 \pm 0.57) \times 10^{-5}\ \mathrm{s^{-1}}, \quad (15)$$

corresponding to a relaxation time of 4.59 ± 0.43 h, which is the value that appears in the persistent-dimer term of Eq. (3). This value is in good agreement with 4.1 h measured by Chann *et al.* [12]. It is smaller than 5.45 h deduced from measurements in our previous work [9]; however, most of this discrepancy can be traced to using different data to calculate the relative contributions of the SR and CSA interactions to the total second moment. Our previous work was done almost exclusively at $B_0=8.0$ T, where we took the measured rate and divided it by the fraction of the second moment that is due to the SR interaction in order to obtain a value appropriate in the low-field limit. This fraction was determined from the measurements of Moudrakovski *et al.* [13] to be 71% at 8.0 T. A similar calculation based on the data presented here [see Eqs. (12) and (13)] yields an 81% contribution for the SR interaction at 8.0 T, which would lower the relaxation time in our previous work [9] to 4.8 h, in much better agreement with the present result.

C. Measured temperature dependence

We performed a series of individual relaxation measurements in temperature range 20–100 °C at 8.0 T for $[G]=0.35$ amagat, well into the density-independent fast-fluctuation limit. Relaxation due to transient dimers is negli-

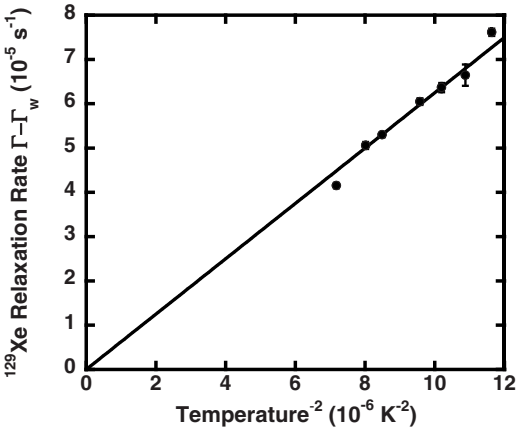

FIG. 3. ^{129}Xe persistent-dimer relaxation rate Γ_p at 8.0 T vs $1/T^2$, where the absolute temperature T ranges between 293 and 373 K. The measured rates were slightly corrected by subtracting the relatively small room-temperature wall-relaxation rate Γ_w. The line is a one-parameter linear fit forced through the origin. Given the theoretical analysis in Sec. II B, this strong dependence of Γ_p on temperature is not well understood.

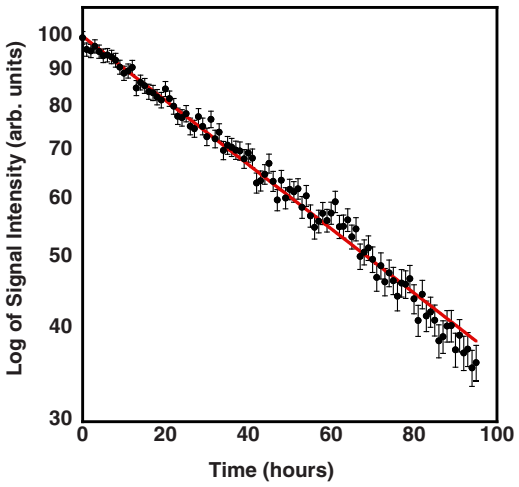

FIG. 4. (Color online) Plot of NMR signal intensity vs time for cell 113B at room temperature in an applied field of 14.1 T. The cell contains xenon at 12.0 mbar and nitrogen at 1.09 mbar. To our knowledge, this is by far the longest gas-phase relaxation time ever recorded for ^{129}Xe and results from the simultaneous suppression of the intrinsic persistent-dimer mechanism and the wall-relaxation mechanism at 14.1 T.

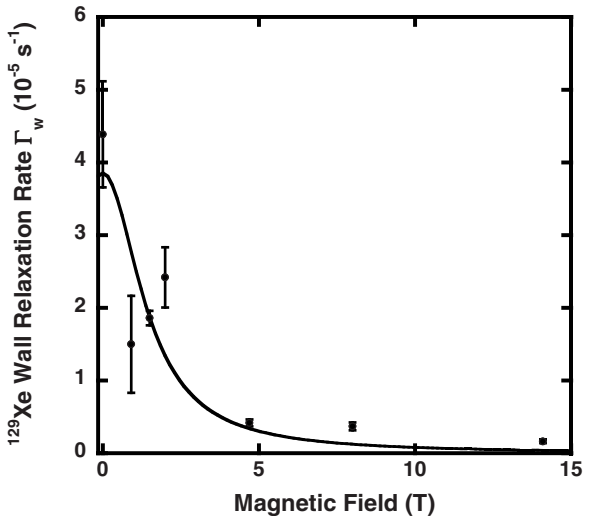

FIG. 5. Room-temperature ^{129}Xe wall-relaxation rate Γ_w as a function of applied magnetic field B_0. The points with small error bars are extracted from the density-dependence curves shown in Fig. 1; the weighted fit to Eq. (16) is almost entirely determined by these points. The other points result from single measurements on pure xenon in the fast-fluctuation limit, where the persistent dimer relaxation rate $\Gamma_{\mathrm{vdW}}^{\mathrm{Xe}}=(6.05\pm0.57)\times10^{-5}$ s^{-1} has been subtracted from the measured relaxation rate. The error propagation from this subtraction leads to the much larger error bars. The fit yields a correlation time for the wall interaction of $\approx$4 ns, consistent with interaction of ^{129}Xe with fluctuating paramagnetic sites on or in the wall coating.

gible for this low density, but the measured rates at all temperatures have been corrected by subtracting the room-temperature wall-relaxation rate at 8.0 T (see Table I). The higher-temperature points are likely over-corrected, since Γ_w should become smaller at higher temperatures due to decreasing residence time on the coating, assuming that this time is governed by an Arrhenius relationship [21]. However, the correction is small in any case, corresponding to a relaxation time of $\approx$75 h, so we use it as a best approximation at all temperatures. The corrected data are plotted in Fig. 3 vs the inverse-squared absolute temperature. The one-parameter least-squares linear fit to this data (forced through the origin) indicates a dependence of the persistent-dimer relaxation rate on $1/T^2$. Our analysis in Sec. II B indicates that Γ_p should be approximately independent of temperature, apart from a possible dependence of the breakup cross section, so this result is somewhat surprising. Ideally, we would have performed these measurements in the low-field limit, but they were instead done at 8.0 T, in order to clearly separate Γ_p from any temperature-dependent wall relaxation. The trade-off is that, in addition to the dominant SR interaction, there is a small contribution from the CSA, which has a different temperature dependence. However, the CSA contribution is only 19% at room temperature (see end of previous section and Fig. 2) and becomes even smaller for $T>293$ K due to the increasing strength of the SR interaction. None of the other parameters having to do with the collision kinetics or the internal molecular states should depend on magnetic field. Hence, these results should be reasonably valid in the low-field limit and contribute to longer overall relaxation times at higher temperatures. Scaling the result for pure xenon in Eq. (15) by $(293\ \mathrm{K})/T^2$ yields a predicted intrinsic maximum T_1 for pure xenon of 7.4 h at $T=100$ °C.

D. Wall relaxation

The extracted wall-relaxation rates Γ_w in Table I decrease dramatically with increasing applied field. At 14.1 T, in the low-density regime where the persistent-dimer rate is highly suppressed, we measured $T_1=99.4$ h for $[G]=0.012$ amagat. The wall-relaxation time extracted from the fit is an extraordinary 174 h. The plot of recorded NMR signal intensity vs time for this measurement is shown in Fig. 4; the slope actually trends slightly downward over the course of this measurement, corresponding to $T_1=105$ h for the first 50 h and $T_1=82$ h for the last 45 h. This may have to do with a gradual increase in oxygen concentration (due to very slow outgassing or leakage) into the cell over the course of the long measurement. If this gradual increase in relaxation rate were due solely to collisions with paramagnetic oxygen atoms, it would correspond to an oxygen partial pressure of $\approx10^{-3}$ mbar [14] developing over the course of the measurement.

Figure 5 shows a plot of Γ_w vs B_0 at room temperature. In an attempt to obtain a more complete picture of the field dependence of Γ_w, data were acquired for three additional values of the applied field B_0 made in an electromagnet (0.91 and 2.0 T) and a Helmholtz pair (2.8 mT). For these three data points, Γ_w was not extracted from a fit. Instead, cell 113B was filled with nearly pure xenon ($\alpha\approx1$) from the xenon polarizer and accumulator to a density $\approx$1 amagat. In this density and magnetic-field regime, the persistent-dimer rate $\Gamma_p=\Gamma_{\mathrm{vdW}}^{\mathrm{Xe}}$. According to Eq. (2), Γ_w was then determined

by subtracting our deduced value of $\Gamma_{\mathrm{vdW}}^{\mathrm{Xe}}$ in Eq. (15) from the measured rate for each of the three additional values of B_0.

We model the high-field wall relaxation as

$$\Gamma_w = M^w\left(\frac{\tau_c}{1+\Omega^2\tau_c^2}\right), \tag{16}$$

where M^w is the second moment of the wall interaction and τ_c^{-1} is its correlation time, presumed to be due to fluctuating paramagnetic spins at the surface. This is a simplified version of the model proposed by Driehuys *et al.* [21] based on the expected field dependence of the relaxation due to the coupling of the ^{129}Xe spin I with a wall spin S [36], which contains additional terms in the power spectrum of Eq. (16) involving the Larmor frequency of the spin S in addition to the ^{129}Xe Larmor frequency Ω. In the range of applied field $B_0 < 10$ mT studied in that work, Driehuys *et al.* [21] were able to fit their relaxation data to a sum of two terms involving protons and paramagnetic sites, respectively, as the spin S. They determined that ^{129}Xe relaxes due to coupling with the protons in the surface coating with an associated correlation time $\tau_c \approx 8$ μs. The proton-induced relaxation, which was directly verified with a double-resonance experiment, cannot be explained by a simple adsorption model; rather, xenon atoms must be trapped within the coating for times $\geqslant 8$ μs. The second term yielded a much shorter correlation time $\tau_c \approx 8$ ns, which is a reasonable relaxation time for paramagnetic surface spins at room temperature.

For the much larger applied fields in our work, the relaxation due to protons is completely suppressed. For relaxation due to paramagnetic sites, the terms in the power spectrum involving the paramagnetic resonance frequency are negligible, due to the $\approx 10^3$ larger gyromagnetic ratio for electrons compared to ^{129}Xe, leading to the simple form of Eq. (16). A least-squares fit of the data to this functional form is also shown in Fig. 5, and yields a correlation time $\tau_c \approx 4$ ns (corresponding to a characteristic decoupling field ≈ 3 T), in reasonable agreement with the predicted correlation time for interaction with paramagnetic spins at the surface or inside the coating.

E. Low-field storage cells

To explore the implications of the above results for a practical low-field hyperpolarized-xenon storage cell at ambient pressures, additional experiments were done at $B_0 \approx 3$ mT at both room temperature and $T = 100$ °C. Again, the flow-through xenon polarizer and accumulator provided nearly pure xenon ($\alpha = 1$), and cells were filled to a density ≈ 1 amagat. We also used three additional alkali-metal-free coated cells. Two of these (designated 105B and 113A) were similar in size to cell 113B; the other was also similar except that its diameter (12.7 cm) is double that of the other cells. The cells all showed increases in the measured relaxation time T_1 of 50–100 % at the elevated temperature. Our results are summarized in Table II, which displays measured relaxation times T_1 and the inferred wall-relaxation times based on subtracting from the measured rate both Γ_p and Γ_t, as calculated from Eq. (3). At the elevated temperature, the rate Γ_p was scaled according to the T^{-2} dependence we observed, while the rate Γ_t was scaled by $T^{-1/2}$. We have estimated the temperature dependence in the case of transient dimers by considering that, in the weak-interaction limit, the probability for a spin transition is approximately proportional to the rate of binary collisions and to the square of the collision duration. Hence, we should have $\Gamma_t \propto 1/v$, where $v \propto T^{1/2}$ is the mean thermal velocity of the xenon atoms. In any case, the correction for Γ_t is $\leqslant 10\%$. It is difficult to extract precise information concerning wall-relaxation times, particularly at the elevated temperature, since Γ_p and Γ_w are comparable at these low fields (unlike at $B_0 = 8.0$ T) and both decrease with increasing temperature (see Sec. IV C above). However, it is clear that a significant improvement was realized for the cell with larger S/V; the measured T_1 in this cell of 5.75 h at $T = 100$ °C is a factor of 2 or more longer than any previously recorded ^{129}Xe relaxation time in the low magnetic fields typical of SEOP.

TABLE II. Low-field relaxation times (in hours) of four cells at both room temperature and 100 °C. The first three have a diameter ≈ 6.7 cm and were measured at $B_0 = 2.8$ mT; the last cell has a diameter ≈ 12.7 cm and was measured at $B_0 = 3.1$ mT. The cells all contained pure xenon at the indicated density (in amagats) provided by a homebuilt flow-through xenon polarizer and accumulator. Uncertainties are given in parentheses for the least significant figure(s). The last two columns show the room-temperature wall-relaxation time derived from subtracting the relevant persistent- and transient-dimer rates [Eq. (3)] from the measured rate. The elevated temperature increases the measured T_1 by 50–100 %.

Cell	[Xe]	T_1 293 K	T_1 373 K	T_1 (wall) 293 K	T_1 (wall) 373 K
105B	1.5(1)	2.40(5)	3.66(11)	5.8(8)	8.7(1.1)
113A	≈1.5	1.30(4)	2.45(5)	1.9(1)	4.0(2)
113B	1.1(1)	2.57(15)	4.53(13)	6.6(1.3)	14.5(3.0)
139	0.7(1)	3.40(22)	5.75(23)	16(7)	35(18)

Cells that are even larger with a correspondingly larger xenon storage capacity are possible; the size will eventually be limited by magnetic field gradients far away from the center of a pair of Helmholtz coils, but this limit is not terribly stringent for xenon. As a guideline, we assume Helmholtz pair of radius (and separation) R and a cell having radius no larger than $R/3$. We have estimated (see the Appendix) the gradient-induced relaxation for such a cell to be

$$\Gamma_g \approx 0.02\frac{D}{R^2}. \tag{17}$$

Although the calculation is done for an ideal Helmholtz geometry (actual gradients are likely to be larger), the estimate in Eq. (17) applies only to the outer edge of a cell whose radius is as large as $R/3$, and so remains fairly conservative for the entire cell. For [Xe]=0.2 amagat at (a conservative estimate of the average density during the filling process), $D = 4.1 \times 10^{-5}$ m^2/s at 100 °C [37]. If we take $R = 0.50$ m, a 0.33-m-diameter spherical cell containing pure xenon should have $\Gamma_g^{-1} \geqslant 84$ h from the gradient mechanism alone; this

time would increase by an order of magnitude as the cell is filled to 1 amagat. Such a cell would have a 19 l storage capacity.

For completeness, we note that dilution of xenon with a second gas lowers the rate Γ_p significantly for those gases that can form and break up persistent Xe_2 dimers with an efficiency comparable to Xe itself. Referring to Eq. (4), the second gas decreases the persistent-dimer lifetime τ_p without changing the fraction of xenon atoms bound in molecules. The effects of adding a second gas were studied thoroughly by Chann *et al.* [12] and in our previous work [9]. Nitrogen has the largest breakup coefficient measured (besides xenon); Γ_p is reduced by about one-third for a 50-50 mixture. We have included the effects of a second gas in our semiempirical formula for the total intrinsic relaxation rate in Eq. (3).

F. Summary

We have presented a systematic study of both intrinsic persistent-dimer relaxation and wall relaxation of ^{129}Xe, including temperature and magnetic-field dependence; we conclude that it should be possible to develop a xenon storage cell that has a measured $T_1 \geqslant 7$ h at 3.0 mT and 100 °C for pure xenon at densities up to a few amagats. These cells are silicone-coated but alkali-metal-free and show relatively long and robust wall-relaxation times of up to tens of hours. They can be utilized in state-of-the-art flow-through xenon polarizers, whereby storage times for polarized xenon can be increased by a factor of 3 or more compared with currently employed cryogenic schemes, and cryogenic storage and associated freeze-and-thaw cycles can be eliminated. We note that if production of pure hyperpolarized xenon is required for a given experiment, then separation of xenon from other gases in the mixture (which comes naturally with cryogenic accumulation) might be a limitation of the room-temperature accumulation scheme proposed here. One approach would be to use the cryogen for gas separation only, followed by immediate volatilization and transfer to a storage cell. However, other cryogen-free separation schemes may be possible: the use of a small gas centrifuge (on the order of 0.1 m-diameter) has already been demonstrated for the continuous separation of methane from CO_2 on the time scale of minutes [38,39]; such a device utilizing suitable materials and/or a surface coating that does not depolarize ^{129}Xe could presumably accomplish continuous separation of xenon from the other much lighter gases typically found in a flow-through polarizer.

ACKNOWLEDGMENTS

We are grateful to D. C. Ailion, M. S. Conradi, and G. Laicher for helpful discussions and to K. Teaford for assistance with cell fabrication. This work was supported by the National Science Foundation Grant No. (PHY-0134980).

APPENDIX: FIELD GRADIENTS IN A HELMHOLTZ-COIL GEOMETRY

Here we derive our worst-case estimate of longitudinal relaxation of ^{129}Xe in xenon gas in a spherical cell of radius no greater than $R/3$ placed at the center of a Helmholtz-coil pair of radius (and separation) R. In the regime where the diffusion time across the cell is much longer than the Larmor period [10], gradient relaxation is given by

$$\Gamma_g = D\frac{|\nabla B_\perp|^2}{B_z^2}, \tag{A1}$$

where B_z is the applied longitudinal magnetic field, $\nabla B_\perp$ is the transverse magnetic field gradient, and D is the Xe diffusion coefficient. The field of a Helmholtz pair along the symmetry axis at some position z away from the isocenter is given by [40]

$$B_z = \frac{\mu_0 NIR^2}{2}\left(\frac{1}{[R^2+(z+R/2)^2]^{3/2}} + \frac{1}{[R^2+(z-R/2)^2]^{3/2}}\right), \tag{A2}$$

where μ_0 is the permeability of free space, N is the number of turns on each coil, and I is the current. Owing to the condition $\nabla \times \mathbf{B} = \mathbf{0}$, we can estimate $\nabla B_\perp \approx \nabla_z B_z$, where

$$\nabla_z B_z = -\frac{3\mu_0 NIR^2}{2}\left(\frac{z+R/2}{[R^2+(z+R/2)^2]^{5/2}} + \frac{z-R/2}{[R^2+(z-R/2)^2]^{5/2}}\right). \tag{A3}$$

Substituting $z=R/3$ into Eqs. (A2) and (A3), we find

$$\frac{\nabla_z B_z}{B_z} = -\frac{18}{2257R}\left(\frac{5(37)^{3/2}-61^{5/2}}{37^{3/2}+61^{3/2}}\right). \tag{A4}$$

Evaluating this expression and inserting the result into Eq. (A1) yields Eq. (17), which provides a worst-case estimate in the sense that it applies strictly only to the outer regions of a cell whose radius is as large as $R/3$; the interior regions of the cell would have a significantly smaller value of Γ_g.

[1] T. G. Walker and W. Happer, Rev. Mod. Phys. **69**, 629 (1997).
[2] S. Appelt, A. B. Baranga, C. J. Erickson, M. Romalis, A. R. Young, and W. Happer, Phys. Rev. A **58**, 1412 (1998).
[3] B. Driehuys, J. Walker, J. Pollaro, G. P. Cofer, N. Mistry, D. Schwartz, and G. A. Johnson, Magn. Reson. Med. **58**, 893 (2007).
[4] L. Schröder, T. J. Lowery, C. Hilty, D. E. Wemmer, and A. Pines, Science **314**, 446 (2006).
[5] S. Pawsey, I. Moudrakovski, J. Ripmeester, L.-Q. Wang, G. J. Exarhos, J. L. C. Rowsell, and O. M. Yaqhi, J. Phys. Chem. C **111**, 6060 (2007).
[6] W. Happer, Rev. Mod. Phys. **44**, 169 (1972).
[7] E. Babcock, B. Chann, T. G. Walker, W. C. Chen, and T. R. Gentile, Phys. Rev. Lett. **96**, 083003 (2006).

[8] E. Babcock, I. Nelson, S. Kadlecek, B. Driehuys, L. W. Anderson, F. W. Hersman, and T. G. Walker, Phys. Rev. Lett. **91**, 123003 (2003).
[9] B. N. Berry-Pusey, B. C. Anger, G. Laicher, and B. Saam, Phys. Rev. A **74**, 063408 (2006).
[10] G. D. Cates, S. R. Schaefer, and W. Happer, Phys. Rev. A **37**, 2877 (1988).
[11] L. D. Shearer and G. K. Walters, Phys. Rev. **139**, A1398 (1965).
[12] B. Chann, I. A. Nelson, L. W. Anderson, B. Driehuys, and T. G. Walker, Phys. Rev. Lett. **88**, 113201 (2002).
[13] I. L. Moudrakovski, S. R. Breeze, B. Simard, C. I. Ratcliffe, J. A. Ripmeester, T. Seideman, and J. S. Tse, J. Chem. Phys. **114**, 2173 (2001).
[14] C. J. Jameson, A. K. Jameson, and J. K. Hwang, J. Chem. Phys. **89**, 4074 (1988).
[15] B. Driehuys, G. D. Cates, E. Miron, K. Sauer, D. K. Walter, and W. Happer, Appl. Phys. Lett. **69**, 1668 (1996).
[16] I. C. Ruset, S. Ketel, and F. W. Hersman, Phys. Rev. Lett. **96**, 053002 (2006).
[17] X. Zeng, Z. Wu, T. Call, E. Miron, D. Schreiber, and W. Happer, Phys. Rev. A **31**, 260 (1985).
[18] G. D. Cates, D. R. Benton, M. Gatzke, W. Happer, K. C. Hasson, and N. R. Newbury, Phys. Rev. Lett. **65**, 2591 (1990).
[19] M. Gatzke, G. D. Cates, B. Driehuys, D. Fox, W. Happer, and B. Saam, Phys. Rev. Lett. **70**, 690 (1993).
[20] N. N. Kuzma, D. Babich, and W. Happer, Phys. Rev. B **65**, 134301 (2002).
[21] B. Driehuys, G. D. Cates, and W. Happer, Phys. Rev. Lett. **74**, 4943 (1995).
[22] X. Zeng, E. Miron, W. A. van Wijngaarden, D. Schreiber, and W. Happer, Phys. Lett. **96A**, 191 (1983).
[23] S. R. Breeze, S. Lang, I. Moudrakovski, C. I. Ratcliffe, J. A. Ripmeester, G. Santyr, B. Simard, and I. Zuger, J. Appl. Phys. **87**, 8013 (2000).
[24] W. A. Fitzsimmons, L. L. Tankersley, and G. K. Walters, Phys. Rev. **179**, 156 (1969).
[25] W. Heil, H. Humblot, E. Otten, M. Schafer, R. Surkau, and M. Leduc, Phys. Lett. A **201**, 337 (1995).
[26] R. E. Jacob, S. W. Morgan, B. Saam, and J. C. Leawoods, Phys. Rev. Lett. **87**, 143004 (2001).
[27] A. Deninger, W. Heil, E. W. Otten, M. Wolf, R. K. Kremer, and A. Simon, Eur. Phys. J. D **38**, 439 (2006).
[28] E. R. Hunt and H. Y. Carr, Phys. Rev. **130**, 2302 (1963).
[29] P. S. Hubbard, Phys. Rev. **131**, 1155 (1963).
[30] H. M. McConnell and C. H. Holm, J. Chem. Phys. **25**, 1289 (1956).
[31] H. W. Spiess, D. Schweizer, U. Haeberlen, and K. H. Hausser, J. Magn. Reson. (1969-1992) **5**, 101 (1971).
[32] F. Reif, *Fundamentals of Statistical and Thermal Physics* (McGraw-Hill, New York, 1965).
[33] M. Hanni, P. Lantto, N. Runeberg, J. Jokisaari, and J. Vaara, J. Chem. Phys. **121**, 5908 (2004).
[34] R. E. Jacob, S. W. Morgan, and B. Saam, J. Appl. Phys. **92**, 1588 (2002).
[35] B. Saam and M. S. Conradi, J. Magn. Reson. **134**, 67 (1998).
[36] A. Abragam, *Principles of Nuclear Magnetism* (Oxford Science, New York, 1961).
[37] J. Kestin, K. Knierim, E. A. Mason, B. Najafi, S. T. Ro, and M. Waldman, J. Phys. Chem. Ref. Data **13**, 229 (1984).
[38] R. van Wissen, M. Golombok, and J. J. H. Brouwers, Chem. Eng. Sci. **60**, 4397 (2005).
[39] M. Golombok and L. Chewter, Ind. Eng. Chem. Res. **43**, 1743 (2004).
[40] P. Lorrain, D. R. Corson, and F. Lorrain, *Fundamentals of Electromagnetic Phenomena* (Freeman, New York, 2000).